

Current control of a modular multilevel converter for HVDC applications



Fernando Martinez-Rodrigo ^{a,*}, Santiago de Pablo ^b, L. Carlos Herrero-de Lucas ^a

^a Electronic Technology Department, University of Valladolid, Industrial Engineering School, Calle Francisco Mendizabal 1, 47014 Valladolid, Spain

^b Electronic Technology Department, University of Valladolid, Industrial Engineering School, Paseo del Cauce 59, 47011 Valladolid, Spain

ARTICLE INFO

Article history:

Received 23 March 2014

Accepted 14 April 2015

Available online 14 May 2015

Keywords:

Current controlled converter

HVDC transmission

Modular multilevel converter (MMC)

Multilevel converters

Offshore transmission

ABSTRACT

Multi-modular converters (MMC) are an emerging and promising option for high voltage direct current (HVDC) transmission, connection of offshore wind farms and FACTS. For such converters, two new strategies for current control are proposed, in which a band is defined around the reference current of the three phases, and modules to be turned ON are chosen to keep the three phase currents within the bands. In the first strategy, only the voltage levels adjacent to the grid voltage level are chosen; this is called “constant excitation” and it is the most appropriate when the number of modules per arm is small. The second strategy uses an excitation proportional to the current error, and it is the most appropriate when the number of modules per arm is great. The theoretical foundation of the strategies and the simulation results within an external active and reactive power control loop are presented. Finally, the current control strategies were applied to HVDC transmission from offshore wind farm to the onshore grid.

© 2015 Elsevier Ltd. All rights reserved.

1. Introduction

The cost of an offshore wind farm (OWF) is mainly composed of wind turbines (30–50%), substation and electricity infrastructure (15–30%), foundations (15–25%) and installation (0–30%) [1]. As a part of the electricity infrastructure, the interest in high voltage direct current (HVDC) transmission has grown lately due to the increase in the construction of OWF. In general, the OWF can be connected to the mains via DC or AC transmission. The presence of power electronic converters makes DC transmission more expensive when the wind farm is near the coast, while the higher number of cables makes the transmission more expensive in AC when it is far from the coast. The boundary between the two situations is about 90 km [2]. Also, the length of AC shielded transmission cables is limited due to their capacitance, responsible for the high reactive power consumption; conversely, DC cables do not need reactive power [3].

Offshore wind farms can have a very large number of high-power turbines (up to 5 MW and even higher). When transmission is done by HVDC, the topology of transmission lines can be: one cable and the return by the earth, two active cables and return

by the earth, one active cable for going and one for the return, and two active cables for going and one for the back. An offshore wind park with HVDC transmission is composed by a low or medium AC generator in the turbine, step-up transformer(s) and electronic converter(s) from AC to DC high voltage. All of them can be built according to several topologies: all the turbines parallelized in low AC voltage + one transformer + one electronic converter, groups of turbines parallelized in low AC voltage + one transformer per group (groups are connected in the high voltage AC) + one converter, groups of turbines parallelized in low AC voltage + one transformer per group + one converter per group (groups are connected in the high voltage DC); other configurations may be found in publications [4,5].

The converters used in HVDC transmission are of two types, while a third type is under investigation and being tested [6]. The two types of converters commonly used are line commutated converter (LCC) [7] and voltage source converter (VSC). The VSC converters can be two-level (2L) or multilevel. Under investigation and experimentation is the modular multilevel converter (MMC) (Fig. 1), first introduced for HVDC applications by Marquardt [8]. The VSC-MMC converters have the following advantages over other topologies used in HVDC transmission [9]:

- 1) The capacitive energy storage is distributed.
- 2) It is a modular topology, so it is easily scalable.

* Corresponding author. Tel.: +34 983423921; fax: +34 983423490.
E-mail address: fer_mart@tele.uva.es (F. Martinez-Rodrigo).

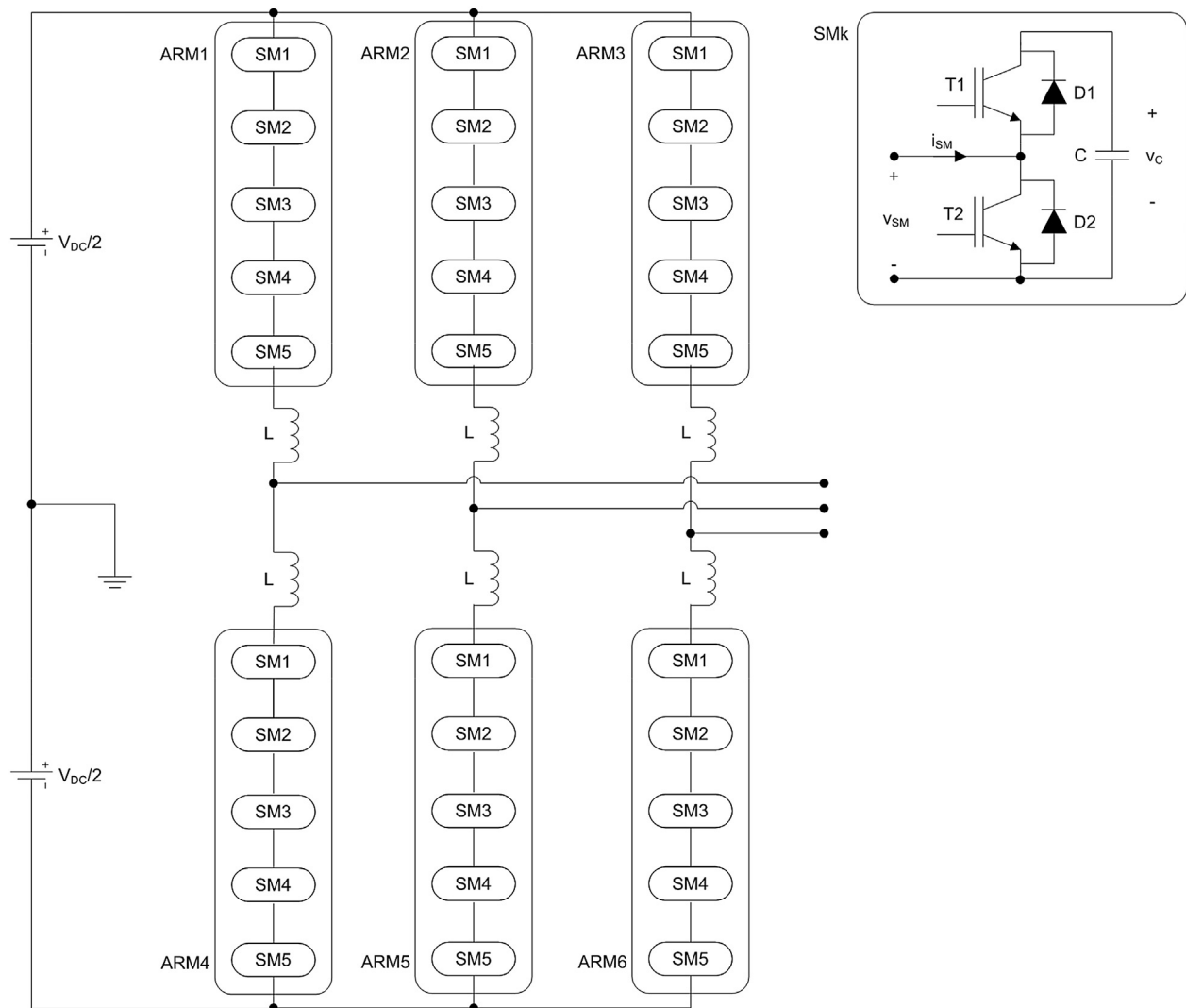


Fig. 1. MMC with five SMs per arm: three phase diagram and structure of each module.

- 3) Due to the high number of levels, filters and transformer may not be necessary.
- 4) The resulting switching frequency is high.

The disadvantage is the large number of semiconductors and drivers that are needed. Furthermore, the energy stored in the capacitors is greater than the conventional two or three level VSC converters. For the reasons stated, it is a very interesting topology, not only for HVDC transmission, but also for other applications including [10]: HVDC transmission, motor drives, STATCOM [11,12], back-to-back converters, wind [13] and solar generation, matrix converters and more.

The MMC technology has been widely accepted in the industry because it allows achieving high power and voltage levels, by employing modules using well-proven technology. It has already been incorporated by the leading manufacturers of HVDC transmission (ABB [14], ALSTOM [15], SIEMENS [16]) as a VSC converter that improves two or three level conventional converters, and it is especially appropriate for offshore wind applications. SIEMENS, for example, has conducted a project to end in 2015, called DoWin2, to make a 135 km HVDC line for connecting one of the largest offshore wind farms in the world.

Expectations of future of HVDC transmission are very large, due to the tendency to lower dependence on fossil fuels and greater penetration of renewable energy, especially offshore wind energy. In this scenario, fault management and operation of multiterminal networks will become very important aspects of HVDC transmission. The superior characteristics of the MMC will make it have a more increasingly importance [17,18].

Some issues that are being investigated on this type of converters are: comparing power losses in semiconductors between MMC-VSC and 2L-VSC converters, modeling the dynamic behavior and steady state, and converter control on balanced and unbalanced systems [19].

Methods of controlling the capacitor voltage are investigated, such as the averaged and balanced control [20], and the predictive control [21]. Equilibration methods that do not need to know the sign of the module current i_{SM} [22] have been presented.

If all the parts of an MMC are accurately simulated, the simulation becomes extremely slow due to the high number of IGBTs. To speed up the simulations, averaged and approximated models, which maintain a high accuracy but take less time to be simulated, are investigated [23,24]. Simplified simulation models are also investigated [25].

To keep the capacitor voltages balanced, the following methods have been proposed: sorting methods depending on the sign of the arm current [9,19], predictive control [21] and techniques to reduce the switching frequency of the modules [26].

To control the voltage and output current of the converter, several possibilities have been presented: multilevel PWM, phase disposition-sinusoidal PWM (PD-SPWM) control and current predictive control.

The multilevel PWM control [9] takes the reference of the output voltage as its starting point; it calculates the average value of the reference voltage in each PWM period, so that the voltage generated by PWM has the same average value over the PWM period; with this criterion, the time that k modules must be ON, and the time that $k+1$ modules must be ON, are calculated. In the example of Fig. 2, the PWM period is T_{PWM} , and the duty cycle of each period (D_1, D_2) is calculated to equal the average value of the output voltage v_o of the converter during this period (v_{o1}, v_{o2}).

The PD-SPWM control [19] is based on comparing the reference of the output voltage with a number of triangular carriers equal to the number n of modules per arm; triangular signals have voltage levels equal to those produced by the n modules and are designed to switch between output voltage levels adjacent to the reference of the voltage (Fig. 3). The carrier phase shift (CPS- PWM) control uses a similar modulation [10].

The predictive current control [21] calculates, every switching period, a cost function for each of the combinations of the modules' state, and selects the state with the lowest cost function; the cost function includes the difference between the reference current and the predicted current, the difference between the capacitors' voltage reference and their predicted value, and the circulating current.

One difference between the MMC and the classical VSC converters is the existence of circulating currents. The equations that allow such currents to be analyzed can be found in Refs. [27]; its control in unbalanced systems is performed in Refs. [28]; and its elimination is studied in Ref. [10].

Other topics that have been investigated are: systems for DC bus protection by means of including thyristors in the modules [29], the influence of sampling frequency and number of modules in the output voltage harmonics [30], modeling and control of MMC under unbalanced systems [31], and the power losses and thermal calculations of semiconductors [9].

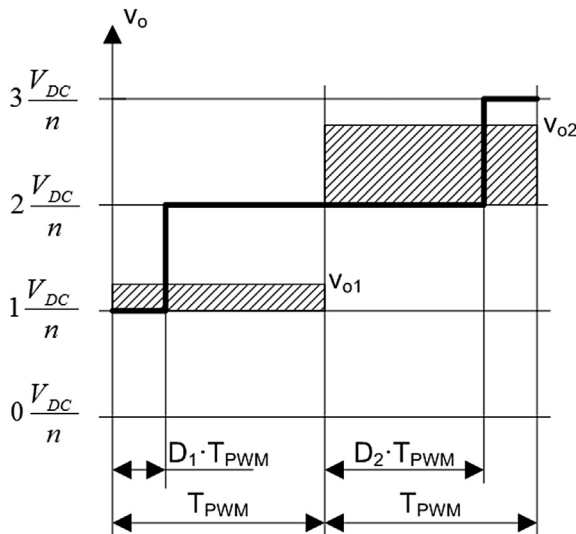


Fig. 2. PWM control to match the average voltage in each period T_{PWM} .

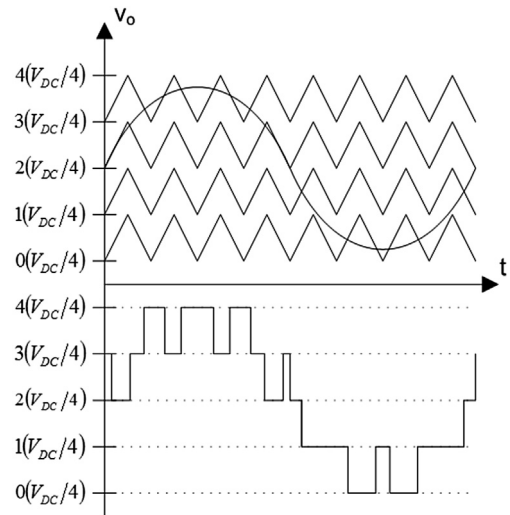


Fig. 3. PD-SPWM control.

In this paper, two novel systems for current control of the MMC in HVDC applications are proposed. The paper is organized as follows. In Chapters 2 and 3, the foundations of the MMC and the method for sorting the SMs to maintain the voltage are, respectively, presented. Chapters 4 and 5 are dedicated to presenting and discussing the two proposed control systems, and the simulation results are included in Chapter 6. Finally, in Chapter 7 one of two new current control strategies has been applied to the HVDC transmission from offshore wind farm to the onshore grid.

2. Fundamentals of MMC

The structure of the MMC can be seen in Fig. 1. It has six arms, each formed by the connection in series of several switching modules (SM) and an inductance. Each SM forming an MMC arm is composed of two IGBTs, two diodes and a capacitor. The SM is in the ON state when the transistor T1 is ON and the transistor T2 is OFF; the SM is OFF when each transistor is in the opposite state (Table 1). When the SM is ON, the module voltage v_{SM} equals the capacitor voltage v_C ; if the module current i_{SM} is positive, the capacitor increases its voltage; while, if i_{SM} is negative, then the capacitor reduces its voltage. When the SM is OFF, the module voltage v_{SM} is zero, and the capacitor voltage remains constant. The voltage of each arm can take discrete values depending on how many SMs are in the ON and OFF states.

The number of modules in the ON state in the upper and lower arms of a phase are referred to as n_{up} and n_{low} , respectively. At all times, the sum of both must equal the total number of modules per arm n , i.e., $n = n_{up} + n_{low}$. Therefore, the capacitor voltage of each module v_C will be regulated to a voltage equal to the DC voltage divided by the number of modules in each arm n , V_{DC}/n .

The output voltage of the first phase v_{oa} (Fig. 4) can be expressed in terms of the variables of the upper or lower arm,

Table 1
SM behavior depending on the status and current.

SM state	T1 state	T2 state	i_{SM}	Δv_C	i_{SM} flows through:	v_{SM}
ON	ON	OFF	>0	$+$	D1	v_C
ON	ON	OFF	<0	$-$	T1	v_C
OFF	OFF	ON	>0	0	T2	0
OFF	OFF	ON	<0	0	D2	0

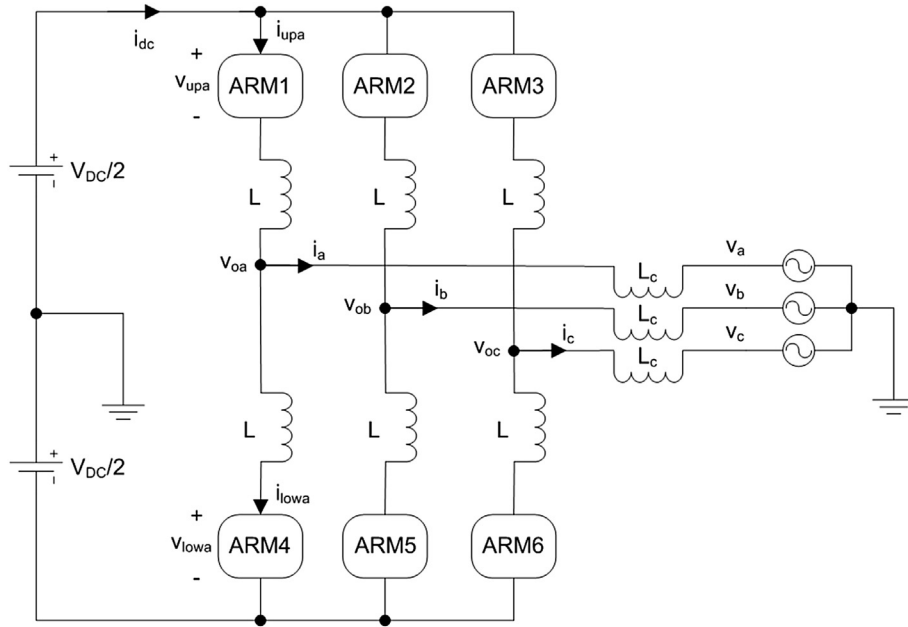


Fig. 4. Connection diagram of MMC to the grid using a coupling inductance.

$$v_{oa} = \frac{V_{DC}}{2} - v_{upa} - L \frac{di_{upa}}{dt} \quad (1)$$

$$v_{oa} = -\frac{V_{DC}}{2} + v_{lowa} + L \frac{di_{lowa}}{dt} \quad (2)$$

The voltage of the arms depends on the number of modules that are ON in each arm:

$$v_{upa} = \sum_{k=1}^n S_{upak} v_{Cupak} \quad (3)$$

$$v_{lowa} = \sum_{k=1}^n S_{lowak} v_{Clowak} \quad (4)$$

where S_{upak} and S_{lowak} is 1/0, depending on the ON/OFF state, respectively, of each SM of the upper and lower arms of phase a, and where v_{cupak} and v_{clowak} are the voltage of each of the capacitors of the upper and lower arms, respectively, of the phase a.

The upper and lower arm currents of phase a (phases b and c are equivalent) are expressed as [19,24]:

$$i_{upa} = \frac{i_a}{2} + \frac{i_{dc}}{3} + i_{za} \quad (5)$$

$$i_{lowa} = -\frac{i_a}{2} + \frac{i_{dc}}{3} + i_{za} \quad (6)$$

where i_{za} is the circulating current of phase a, and its expression is:

$$i_{za} = \frac{i_{upa} + i_{lowa}}{2} - \frac{i_{dc}}{3} \quad (7)$$

The sum of the circulating currents of the three phases is zero:

$$i_{za} + i_{zb} + i_{zc} = 0 \quad (8)$$

3. Output voltage control

The output voltage of each arm v_{oabc} is controlled by the ON and OFF connection of SMs in the upper and lower arms of each phase. If each arm has n modules, each SM will have a capacitor voltage approximately equal to V_{DC}/n . The total number of modules in each phase that must always be ON is n ; therefore, the sum of ON modules of the upper and lower arms must be n , $n = n_{up} + n_{low}$.

If the arm inductances have a small value L , the voltage drop across these inductances is small with respect to the module voltages. Then, the output voltage of each branch v_{oabc} can only take $n+1$ discrete values, where n is the number of modules on each arm. For example, if n is 5 (Table 2), the number of v_{oabc} values is 6: $\{-V_{DC}/2+0v_c; \dots; -V_{DC}/2+5v_c\}$. In Table 2, the number of modules in ON in the upper arm n_{up} and in the lower arm branch n_{low} are indicated in each case.

In the upper/lower arm of each phase, n_{up}/n_{low} modules must be set at ON. Since there are n modules in each arm, which n_{up}/n_{low} modules are to be turned ON must be chosen. For this, an algorithm for sorting the SM voltages is usually chosen in the literature; if the arm current i_{upa}/i_{lowa} is positive, then the modules with a lower voltage are chosen, resulting in the capacitors being charged; if the arm current is negative, then the SMs with higher voltage are selected to discharge the capacitors. This strategy keeps the capacitor voltages stable at around V_{DC}/n . Fig. 5 shows an example of the sorting of a 5 modules arm ($n = 5$) when $n_{up} = 3$; the sorting when the arm current is positive and when it is negative has been included.

Table 2
Levels of output voltage v_{oabc} .

n_{up}	n_{low}	v_{oabc}
5	0	$-V_{DC}/2+0v_c$
4	1	$-V_{DC}/2+1v_c$
3	2	$-V_{DC}/2+2v_c$
2	3	$-V_{DC}/2+3v_c$
1	4	$-V_{DC}/2+4v_c$
0	5	$-V_{DC}/2+5v_c$

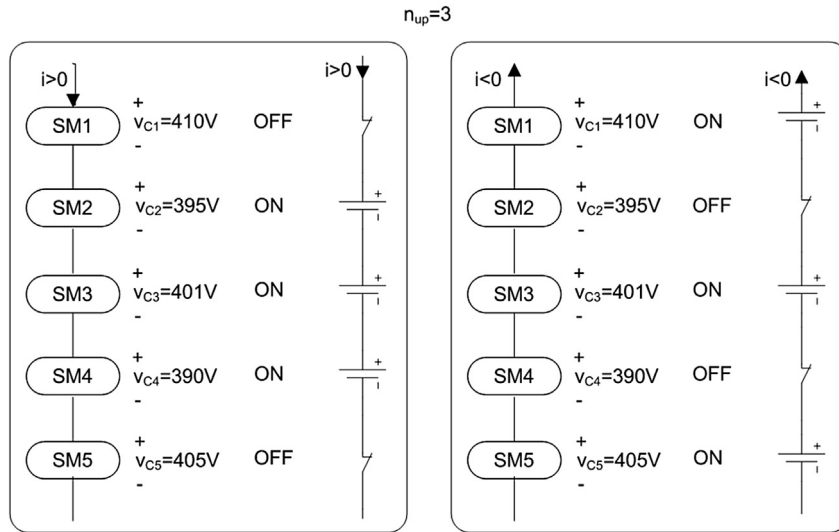


Fig. 5. Example of SMs voltage sorting for $n_{up} = 3$.

4. Current control with constant excitation

The control of MMC for connection to the mains through a coupling inductance is presented. The power scheme can be seen in Fig. 4, where the SMs are grouped into a block called “ARM”.

The connection to the mains can be voltage controlled or current controlled; the second case is presented in this article. Any converter control has two degrees of freedom, i.e., two variables can be controlled independently. The variables chosen to be controlled are the active P and reactive Q powers exchanged with the grid (Fig. 6). Two PI regulators are used to control P and Q, whose outputs are the current references in direct i_d^* and quadrature i_q^* axes with respect to the grid voltage vector v_{abc} ; from these, the reference current of the three phases i_{abc}^* are obtained. The angle θ for the Park transformation is obtained from the network grid voltages v_{abc} , and the values of P and Q are obtained from the grid currents i_{abc} and voltages v_{abc} .

The angle θ is obtained by means of a dq-PLL [32] from the grid voltages v_{abc} (Fig. 7). When the PI block reduces to zero the grid

voltage quadrature component v_q , then the angle θ generated by the PLL is correct. The input ω_{offset} is used to reduce the synchronization time.

The output voltage of each arm v_{oabc} can only take $n+1$ different values, as could be seen in Table 2 and Fig. 8c for $n = 5$. The relationship between this voltage and the number of ON modules in the lower arm n_{low} is:

$$v_o = -\frac{V_{DC}}{2} + n_{low}v_C \tag{9}$$

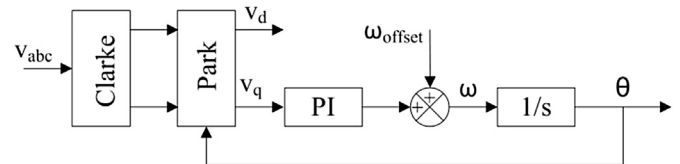


Fig. 7. Scheme of the dq-PLL.

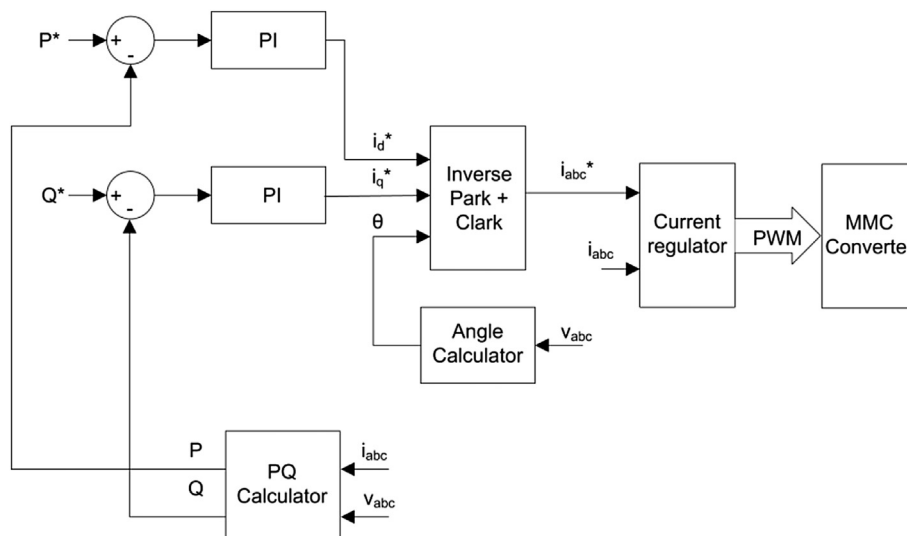


Fig. 6. Control Scheme: regulators of active P and reactive Q power, and current controller.

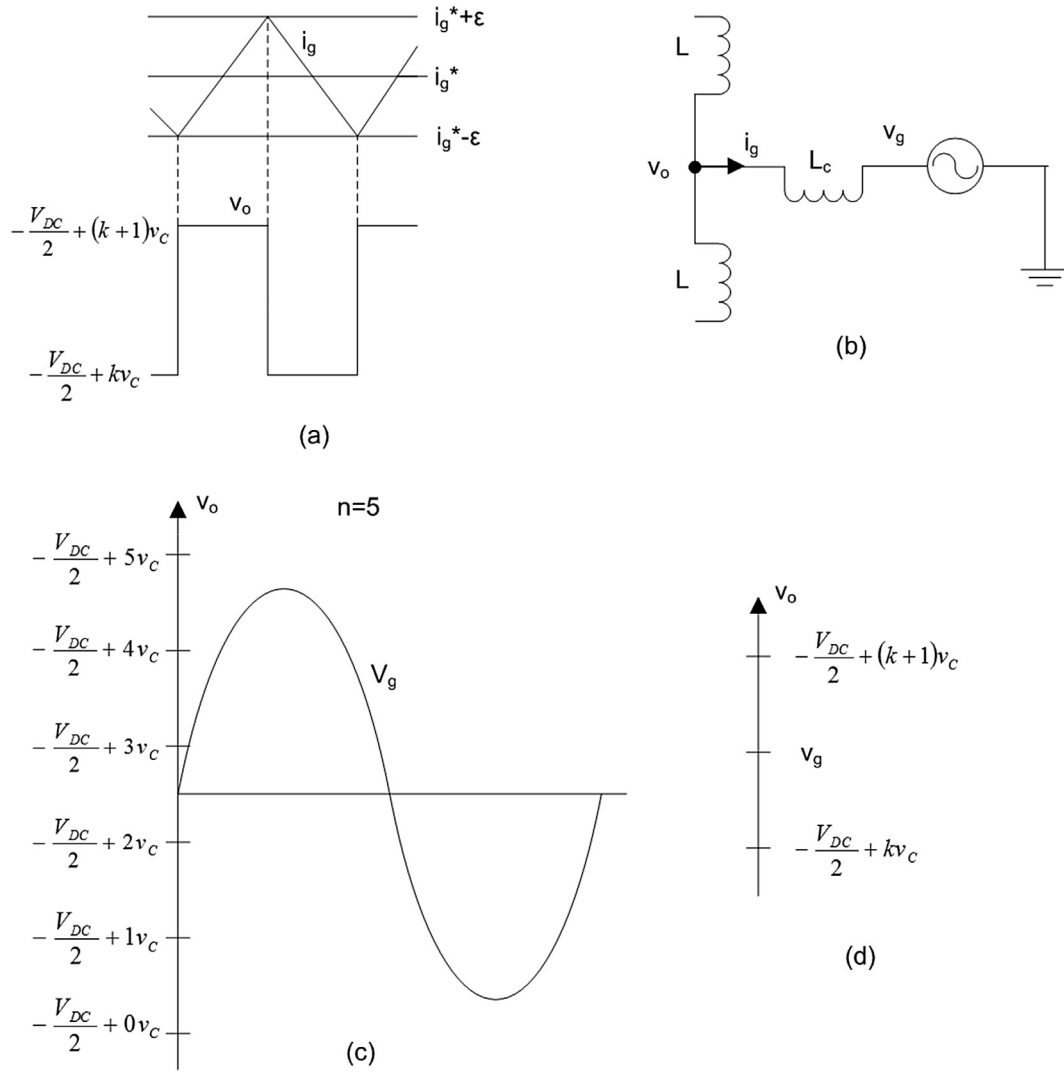


Fig. 8. Constant excitation current regulator: (a) control of grid current i_g within an ϵ band around its reference value i_g^* , (b) grid connection of each phase, (c) values that v_o and v_g can take for $n = 5$, (d) v_o values adjacent to v_g value.

In the current control, the current phase i_g ($g = a,b,c$) is maintained within a band value ϵ around the current reference i_g^* [$i_g^* - \epsilon; i_g^* + \epsilon$] (Fig. 8a), by controlling the voltage at the center point of the arm v_o (Fig. 8b). The coupling inductance current i_g depends on the voltage difference between its ends ($v_o - v_g$), $\Delta i_g = \frac{1}{L_c} \int (v_o - v_g) dt$, where the voltage v_o can only take $n+1$ different values, as can be seen in Fig. 8c for $n = 5$. To control the current i_g , the next to the grid voltage v_g ($g = a,b,c$) higher ($-\frac{V_{DC}}{2} + (k+1)v_c$) and lower ($-\frac{V_{DC}}{2} + kv_c$) values of v_o are chosen (Fig. 8d). To obtain these v_o voltages, a number of $n_{low} = k$ SMs must be connected to ON. The reason for choosing these values of v_o is to reduce the inductance L_c , taking advantage of having a multi-level converter.

This procedure, which employs only v_o values immediately above and below v_g , will be called the constant excitation algorithm; its diagram can be seen in Fig. 9. The parameter k is calculated as:

$$k = \text{floor} \left(\left(v_g + \frac{V_{DC}}{2} \right) / v_c \right) \quad (10)$$

where “floor” means: round to an integer towards negative infinity.

4.1. PI controller tuning procedure

Active and reactive power can be calculated, based on the d-axis component of the grid voltage v_d and the d- and q-axis components of the grid current i_d and i_q as [21]:

$$P = \frac{3}{2} v_d i_d \quad (11)$$

$$Q = -\frac{3}{2} v_d i_q \quad (12)$$

As the grid voltage can be considered constant, its component v_d can be considered constant as well. If the active power regulator is adjusted to be significantly slower than the current regulator, then for the purposes of PI controller design can be considered $i_d = i_d^*$, and (11) becomes:

$$P = \frac{3}{2} v_d i_d^* \quad (13)$$

Then, the design of the active power PI controller (Fig. 10) can be done by replacing the PI block by an integral block $k_{i,p}/s$. The closed loop transfer function is:

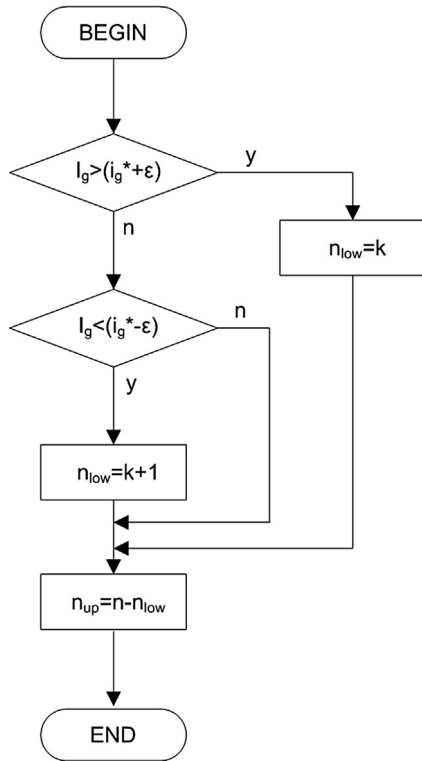


Fig. 9. Algorithm of the constant excitation current regulator.

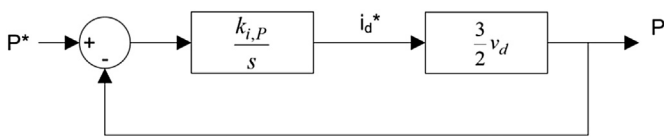


Fig. 10. Active power control scheme.

$$\frac{P(s)}{P^*(s)} = \frac{1}{1 + \frac{1}{k_{i,P} \frac{3}{2} v_d} s} \quad (14)$$

This is a first order transfer function, whose time constant T_1 is:

$$T_1 = \frac{1}{k_{i,P} \frac{3}{2} v_d} \quad (15)$$

The tuning of the active power regulator consists in choosing a value of T_1 much smaller than the time variation of the current control loop. The current regulator is nonlinear and very fast; then the variation time of the current i_a will be estimated. According to Fig. 4, for a small time, the coupling inductance equation can be written as:

$$\Delta t = \frac{L \Delta i_a}{v_{oa} - v_a} \quad (16)$$

The voltage across the inductance ($v_{oa} - v_a$) can be replaced by half an interval of the converter output voltage $V_{DC}/2n$. The value Δi_a can be replaced by the peak value $i_{a,peak}$, and this, according to Clarke and Park transformations, by $i_{d,max}$. Then, the time constant T_1 of the active power regulator must be chosen to be much smaller than the time Δt .

As an example, the integral constant $k_{i,P}$ of the active power regulator will be calculated for data to be employed in simulations

Table 3
Simulation parameters.

n	5	10
T_s	5 μ s	5 μ s
T_{cr}	15 μ s	15 μ s
T_{PQR}	120 μ s	120 μ s
V_{DC}	4 kV	4 kV
C	30 mF	60 mF
L	375 μ H	375 μ H
$V_{g,rms}$	1250 V	1250 V
ε	3 A	3 A
L_c	3 mH	3 mH
P^*	370 kW	370 kW
Q^*	-370 kVAR	-370 kVAR
$k_{p,P}$	0	0
$k_{i,P}$	0.1	0.1
$k_{p,Q}$	0	0
$k_{i,Q}$	-0.1	-0.1
k_i	0.5	0.5
$k_{p,PLL}$	0.2	0.2
$k_{i,PLL}$	2	2

of section 6 (Table 3). The maximum value of current $i_{d,max}$ is calculated by (11) as:

$$i_{d,max} = \frac{P_{max}}{\frac{3}{2} v_d} = \frac{370 \cdot 10^3}{\frac{3}{2} 1250 \sqrt{2}} = 139.5 \text{ A} \quad (17)$$

The time required for a current variation $\Delta i_a = i_{d,max}$ is calculated from (16),

$$\Delta t = \frac{L i_{d,max}}{\frac{V_{DC}}{2n}} = \frac{375 \cdot 10^{-6} \cdot 139.5}{\frac{4 \cdot 10^3}{2 \cdot 5}} = 131 \mu\text{s} \quad (18)$$

The time constant T_1 should be chosen at least 10 times greater than Δt , i.e. $T_1 = 1.31$ ms. Then, the regulator integral constant is, using (15),

$$k_{i,P} = \frac{1}{T_1 \frac{3}{2} v_d} = \frac{1}{0.00131 \frac{3}{2} 1250 \sqrt{2}} = 0.288 \quad (19)$$

In the simulation, value $k_{i,P} = 0.1$ has been used, which is somewhat lower than calculated, since it was not such a quick response needed for active power P.

Reactive power regulator is calculated entirely similar. A negative value should be employed in the integral regulator constant, $k_{i,P} = -0.1$, to compensate the negative sign on the calculation of Q, as shown in (12).

5. Current control with excitation proportional to the error

When the number n of SMs per arm is high, the voltage of each SM v_{SM} is relatively small and may be insufficient to effectively lead the current phase i_g to the reference value i_g^* . The current i_g increases or decreases, depending on whether the voltage across the inductor ($v_o - v_g$) is positive or negative, respectively. When the number of modules is high and constant excitation strategy is used, the inductance voltage may be insufficient at times, making it necessary to increase the converter phase voltage v_o . For this, a new strategy has been developed in which the voltage v_o does not take, as possible values, only those adjacent to the grid voltage v_g , but can take more distant values to increase the inductance voltage and, thus, the speed of the current i_g variation.

The proposed algorithm for current control takes, as its starting point, the one proposed in Fig. 9, but it can generate voltages v_o more distant from v_g when necessary (Fig. 11a). When the phase

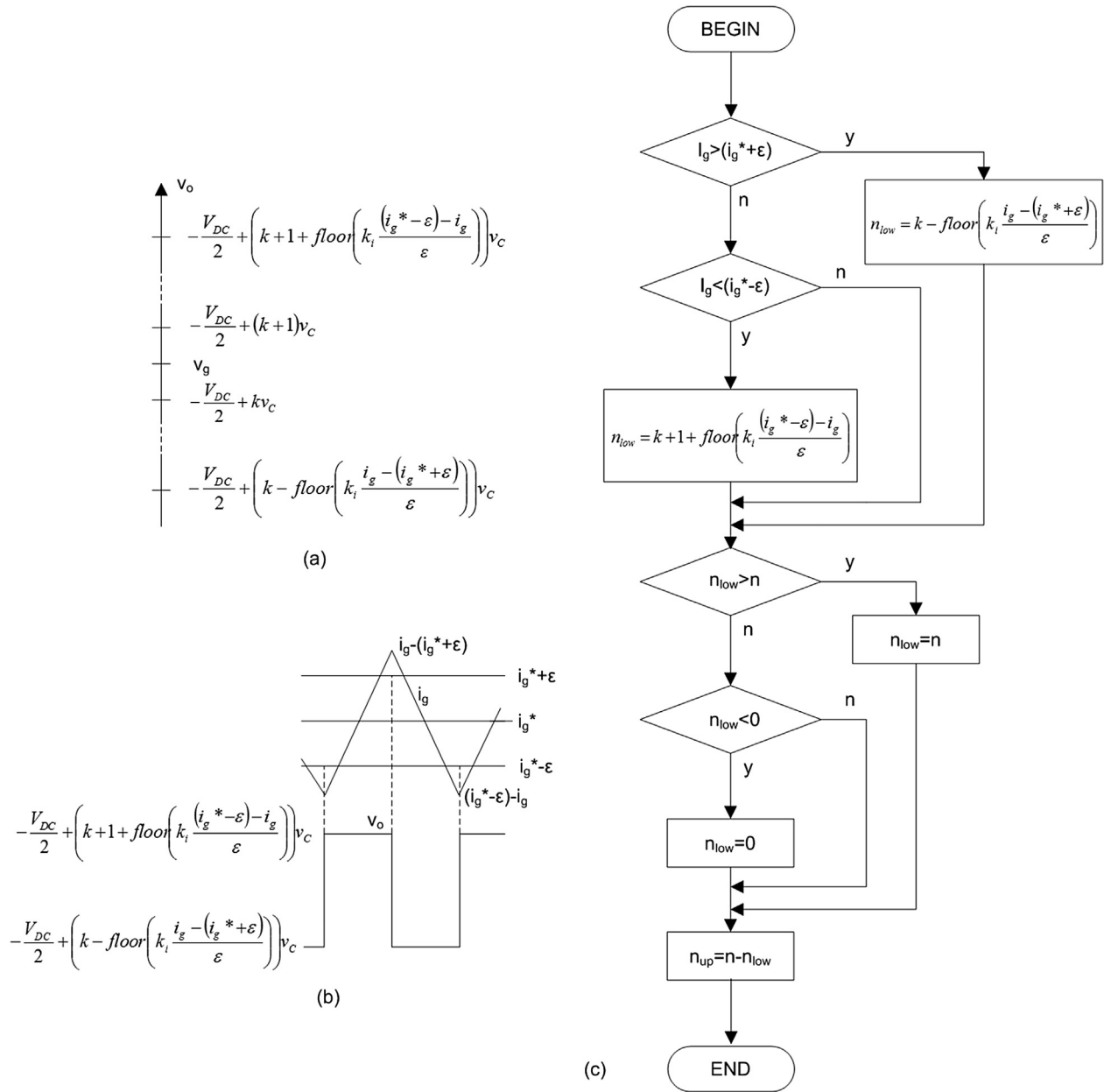


Fig. 11. Algorithm of current control with excitation proportional to the error: (a) discrete levels of v_o , (b) current i_g and voltage v_o (c) diagram of the algorithm.

current i_g moves away from the reference value i_g^* , a value greater than ε , a higher excitation enters v_o to increase the ability to push i_g towards i_g^* . The value of v_o to be introduced will have a distance from v_g proportional to the magnitude that i_g has left the band (see Fig. 11b), while respecting the quantification of voltage v_o imposed by the modules. The constant k_i is used to relate the excitation with the error in the current. Thus, the values used for v_o are:

$$v_o = -\frac{V_{DC}}{2} + \left(k + 1 + \text{floor}\left(k_i \frac{(i_g^* - \varepsilon) - i_g}{\varepsilon}\right)\right) v_c \quad (20)$$

and

$$v_o = -\frac{V_{DC}}{2} + \left(k - \text{floor}\left(k_i \frac{i_g - (i_g^* + \varepsilon)}{\varepsilon}\right)\right) v_c \quad (21)$$

and are used, respectively, when current i_g is over or below the band ε around i_g^* .

The algorithm diagram can be seen in Fig. 11c. At the top, the quantized value of v_o is determined according to the current above the band, below the band or remaining within the band. The bottom is a limitation of n_{low} value, which should be in the range $[0; n]$.

6. Simulation results

The behavior of the current control system with constant excitation and excitation proportional to the error was simulated. In the first case, the number of SMS in each arm was $n = 5$, and in the second case $n = 10$. The design goals were to regulate the active P and reactive Q powers exchanged with the grid, and meet the requirements of current harmonics injected to the grid.

The simulation was performed by means of Matlab/Simulink, using exact models of each SM and replacing the IGBT by ideal switches. The parameters used in the simulation of the two control strategies are the same (Table 3); in the case of the capacitor, the values are different because what has been matched is the equivalent capacitance of each arm. The sampling period T_s used in the simulation was $5 \mu s$. The power regulators had a period T_{PQR} of $120 \mu s$, i.e., to produce a new reference value of i_d^* and i_q^* every $120 \mu s$.

The current regulator takes a decision every $15 \mu s$ (T_{Cr}). This decision may be to change the output voltage level v_{oabc} , if the phase current i_{abc} has left the band ϵ , or to maintain the output voltage level otherwise. This does not mean that the output voltage v_o has a switching frequency of 33.3 kHz ($1/2 \cdot 15 \mu s$), since, in many cases, the current controller does not change the output voltage v_o because the current phase i_{abc} is within the band ϵ . Graphs are included for the trigger signals to evaluate the IGBT switching frequency; it is found that frequencies are allowable for high power IGBTs.

According to relevant standards of connecting generators to the grid, the total harmonic distortion (THD) of the current injected into the grid should be less than 5% [33]. The specific limits of each harmonic are in Table 4. These data will be used to analyze the simulation results of the converters.

6.1. Current control with constant excitation and $n = 5$

The simulation results of the controller with five modules in each arm, $n = 5$, and current control with constant excitation are presented. The converter output currents i_{abc} and voltages v_{oabc} can be seen in Fig. 12. These voltages have 6 voltage levels ($n+1$) which are not constant as they have a ripple due to the voltage drop produced by the arm currents i_{upa} and i_{lowa} (Fig. 13) in the inductance L . The voltages v_{oabc} take values immediately above and below the grid voltage v_{abc} . The currents i_{abc} perfectly follow their reference values i_{abc}^* .

The harmonic content of the phase currents i_{abc} (Fig. 14) meets the requirements for the harmonics indicated in Chapter 6 and

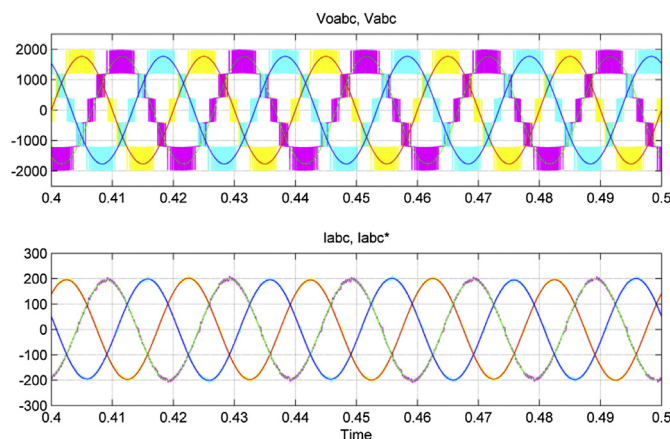


Fig. 12. Converter output voltages v_{oabc} , grid voltages v_{abc} , converter output currents i_{abc} and reference values of the converter output currents i_{abc}^* .

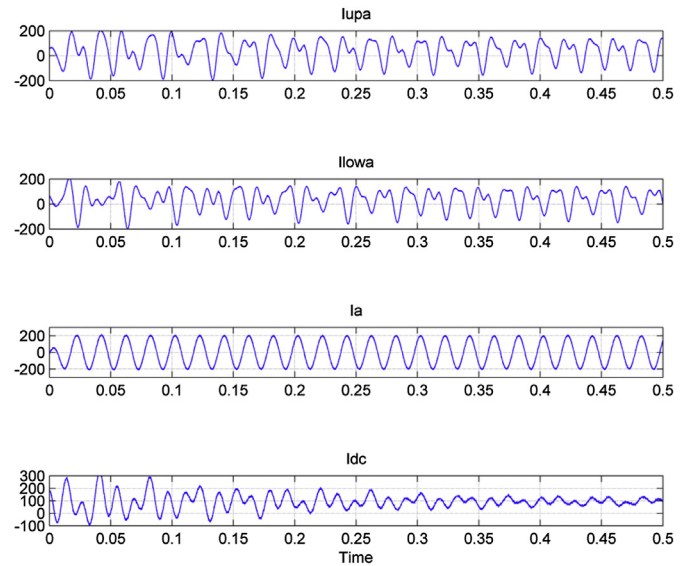


Fig. 13. Higher arm current i_{upa} , lower arm current i_{lowa} , phase current i_a and DC source current i_{dc} .

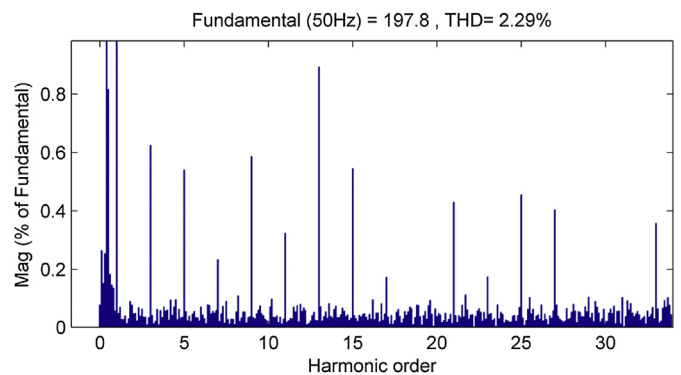


Fig. 14. Harmonics of phase current i_a .

Table 4
Maximum levels of current harmonics in the grid connection of generators.

Odd harmonics	Maximum value
3–9	4%
11–15	2%
17–21	1.5%
23–33	0.6%

Table 4. The active P and reactive Q power follow their reference values P^* and Q^* of 370 kW and -370 kVAR , respectively (Fig. 15).

In Fig. 16, the five SM voltages of the upper arm v_{cup} (top figure) and the lower arm v_{clow} (bottom figure) are seen superimposed. The voltage variation is due to the currents in the upper i_{upa} and lower i_{lowa} arms (Fig. 13). The sorting algorithm of the SMs is able to keep the voltage of the five capacitors of each branch, v_{cup} and v_{clow} , balanced at all times. Variations in the voltage capacitors, v_{cup} and v_{clow} , could be reduced by increasing the SM capacitor C . The output currents i_{abc} have reduced harmonic content (Fig. 14), meeting the requirements for THD (5%) and individual harmonics (Table 4).

The current of the DC source i_{dc} (Fig. 13) has a positive mean value, since this source must provide positive active power. The circulating current i_{za} (Fig. 17) was calculated by (7) and has twice the grid frequency (100 Hz).

The IGBT trigger signal can be seen in Fig. 18; it has a switching period ranging from $60 \mu s$ to $350 \mu s$, which is large enough to employ high power IGBTs.

6.2. Current control with excitation proportional to the error and $n = 10$

The simulation results of the converter with ten modules on each arm, $n = 10$, and current control with excitation proportional

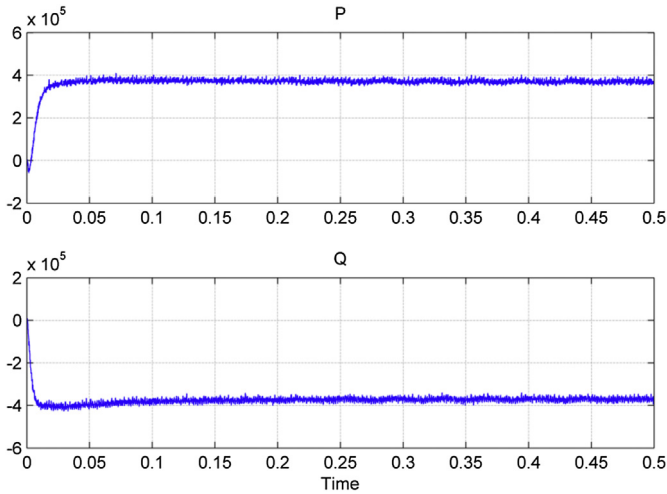


Fig. 15. Active P and reactive Q power exchanged between the converter and the grid.

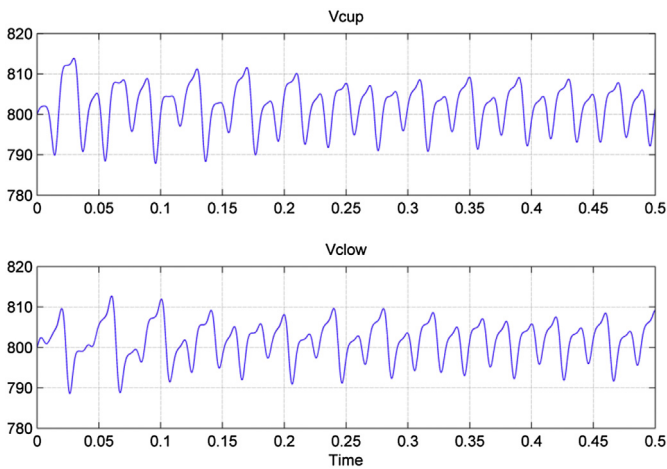


Fig. 16. Capacitor voltages of the five upper v_{cup} and lower v_{clow} SMs of the phase a arms. In the upper figure, the five capacitor voltages are superimposed, and in the lower figure, the five capacitor voltages are also superimposed.

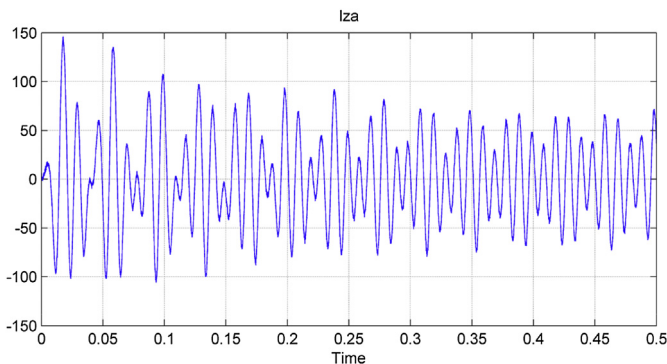


Fig. 17. Circulating current of phase a i_{za} .

to the error are presented. The output currents i_{abc} and voltages v_{oabc} can be seen in Fig. 19. The voltages have 11 levels ($n+1$) which are not constant as they have a ripple due to the voltage drop produced by the arm currents i_{upa} and i_{lowa} (Fig. 20) in the inductance L . Unlike what happened when the excitation was constant, the voltages v_{oabc} not only take on the values immediately above

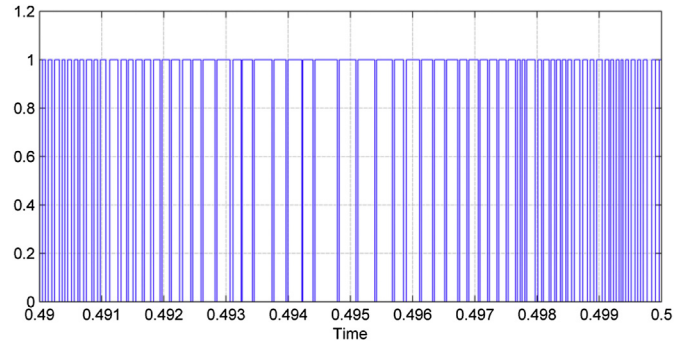


Fig. 18. Trigger signal of SM1 of arm 1.

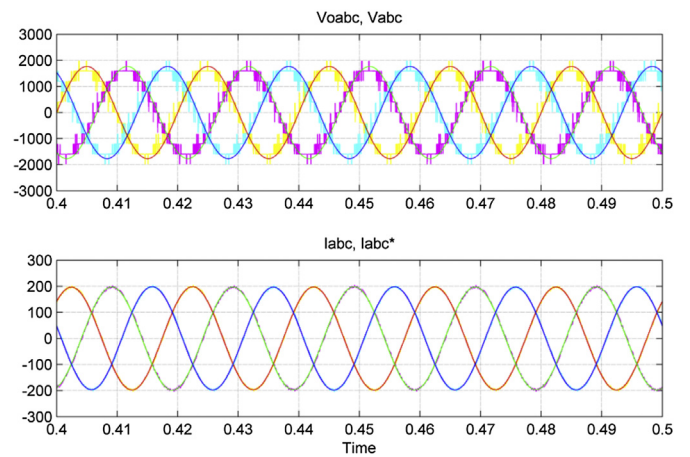


Fig. 19. Converter output voltages v_{oabc} , grid voltages v_{abc} , converter output currents i_{abc} and reference values of the converter output currents i_{abc}^* .

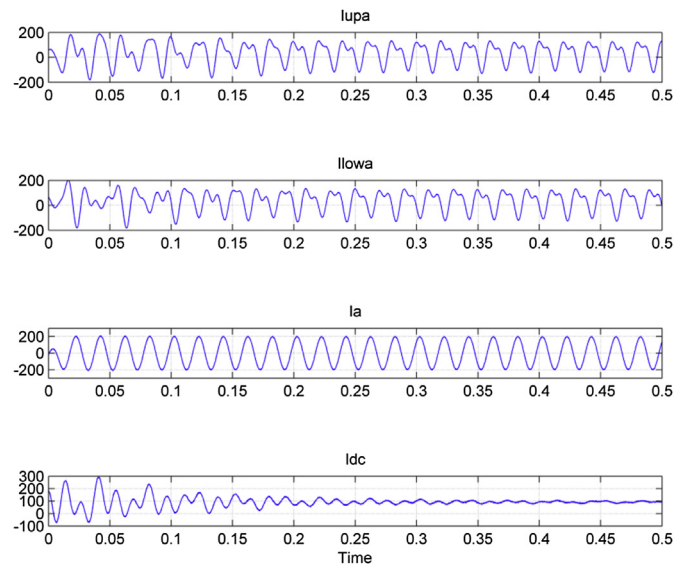


Fig. 20. Higher arm current i_{upa} , lower arm current i_{lowa} , phase current i_a and DC source current i_{dc} .

and below the grid voltages v_{abc} , but they also take values proportional to the current error, where the proportionality constant k_i was chosen by trial and error to minimize the current harmonics. This has ensured that the currents i_{abc} perfectly follow their reference values i_{abc}^* .

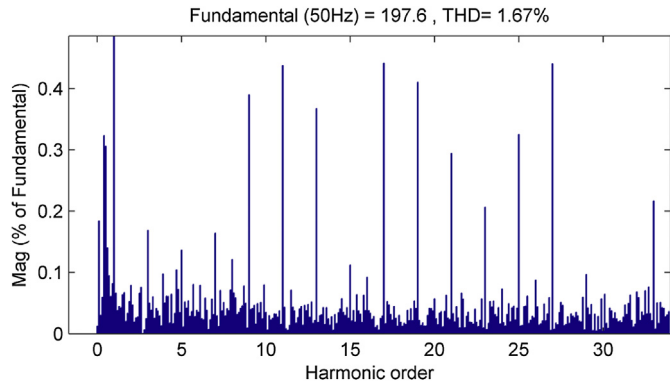


Fig. 21. Harmonics of phase current i_a .

The harmonic content of the phase currents i_{abc} (Fig. 21) meets the requirements for the harmonics indicated in Chapter 6 and Table 4; the THD is lower than 5% and the individual harmonics are under the limits indicated in Table 4. The active P and reactive Q power follow their reference values P^* and Q^* of 370 kW and -370kVAR , respectively (Fig. 22).

In Fig. 23, the ten SM voltages of the upper arm v_{cup} (top figure) and the lower arm v_{clow} (bottom figure) are displayed superimposed. The voltage variation is due to the currents in the upper i_{upa} and lower i_{lowa} arms (Fig. 20). The sorting algorithm of the SMs is able to keep the voltage of the ten capacitors of each branch, v_{cup} and v_{clow} , balanced at all times. The variations of voltage in the capacitors, v_{cup} and v_{clow} , have been reduced with respect to Fig. 16 by increasing the capacitance C of the SMs.

The current of the DC source i_{dc} (Fig. 20) has a positive mean value, since this source must provide positive active power. The circulating current i_{za} (Fig. 24) was calculated by (7) and has twice the grid frequency (100 Hz).

The IGBT trigger signal can be seen in Fig. 25; it has a switching period ranging from 80 μs to 500 μs .

6.3. Comparison of the two control strategies using performance indices

The two control strategies will be compared using performance indices applied to the error signal of the active and reactive power PI regulators. The indices chosen are integral square error

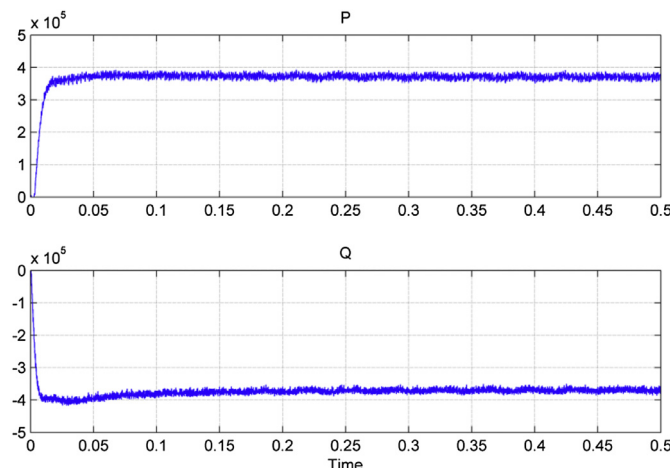


Fig. 22. Active P and reactive Q power exchanged between the converter and the grid.

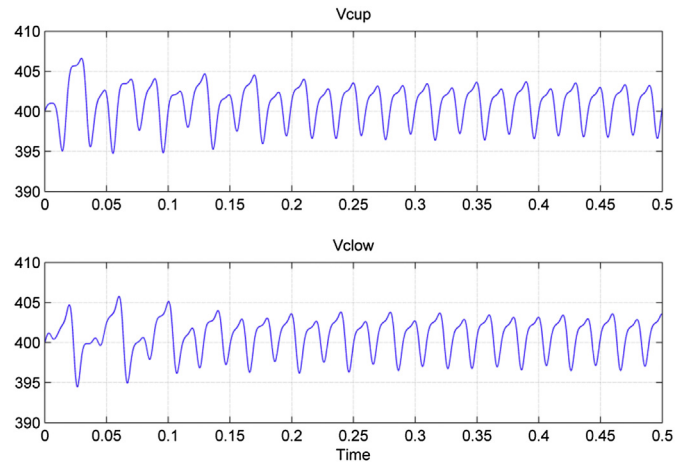


Fig. 23. Capacitor voltages of the ten upper v_{cup} and lower v_{clow} SMs of the phase a arms. In the upper figure, the ten capacitor voltages are superimposed, and in the lower figure, the ten capacitor voltages are also superimposed.

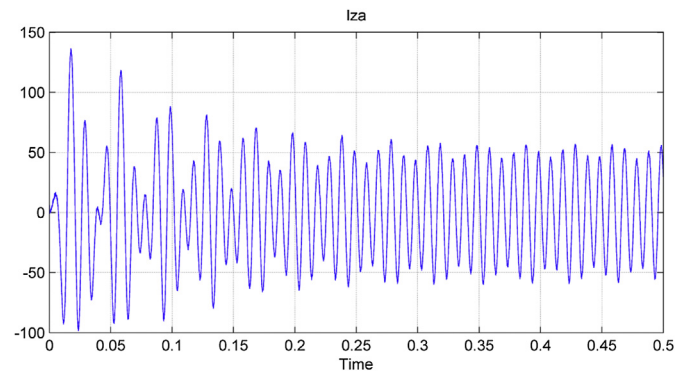


Fig. 24. Circulating current of phase a i_{za} .

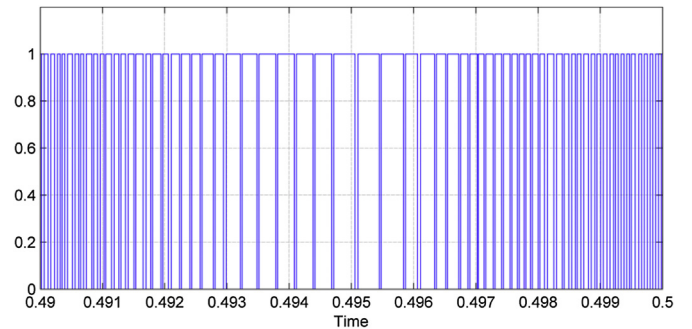


Fig. 25. Trigger signal of SM1 of arm 1.

(ISE) and integral of the absolute magnitude of error (IAE), which are defined as:

$$ISE = \int e^2 dt \tag{22}$$

$$IAE = \int |e| dt \tag{23}$$

To compare the two control strategies, the same simulation parameters have been used in both (Table 3). Performance indices obtained in the simulations are included in Table 5.

Table 5
Performance indices ISE and IAE for active and reactive power regulators.

n	P		Q	
	ISE	IAE	ISE	IAE
5	$8.87 \cdot 10^8$	6678	$3.64 \cdot 10^8$	6516
10	$8.64 \cdot 10^8$	6074	$3.34 \cdot 10^8$	5430
Index reduction (%)	2.59	9.04	8.24	16.7

All indices indicate that error in active and reactive power is lower in the second strategy, and that the error is lower in the reactive power than in the active power.

7. Application on an offshore wind farm

In this section, the first control strategy (control with constant current excitation) is applied to an offshore wind farm. Two MMCs with five ($n = 5$) SMs per arm are used (Fig. 26); the first MMC is used to convert the wind farm AC voltage to DC voltage; this converter is called wind farm MMC (WF-MMC); the second converter is used to convert the DC voltage to AC voltage on the side of the onshore grid, which is called grid connection MMC (GC-MMC). The WF-MMC is in the sea beside the wind farm, the DC cables are underwater and the GC-MMC is on land. The wind farm simulated has a power rating of 9 MW and a phase-to-phase AC voltage of 25 kV rms.

Both MMCs have the same topology as the converter of Fig. 4, with the only difference that DC voltage sources $V_{DC}/2$ are replaced by capacitors C_{DC} , because the converter must be voltage source topology.

The resistances R of the DC cables have been included. Lower cable resistance could be eliminated if the current returns through the seawater.

Each MMC has two PI regulators to control two variables (Fig. 27). In the WF-MMC, the variables that are controlled are the active P_{WF} and the reactive Q_{WF} power (as in Fig. 6), therefore, the reference variables are P_{WF}^* and Q_{WF}^* (Fig. 26). In the GC-MMC, the variables which are controlled are the converter DC voltage V_{DC} and the reactive power Q_{GC} . The Q_{GC} regulator is like that of Fig. 6. The active power regulator of Fig. 6 has been replaced by the DC voltage

regulator, in which the variables P^* and P have been replaced by V_{DC}^* and V_{DC} , respectively; the control variable of this controller is the current i_{dGC}^* .

The active power of both MMCs, P_{WF} and P_{GC} , is considered positive when the power goes from the DC side to the AC side (Fig. 26), i.e., during normal operation, power P_{WF} is negative because the wind farm delivers power to the WF-MMC, and P_{GC} power is positive because active power is transmitted to the terrestrial grid.

The WF-MMC is connected to the wind farm via 12 mH coupling inductances (Table 6), which have higher value than those used in Table 3 because in this simulation the AC and DC voltages are greater. For the same reason, coupling inductances between the GC-MMC and the distribution grid are also 12 mH.

The proportional $k_{p,VDC}$ and integral $k_{i,VDC}$ constants of the DC voltage controller have negative values since the current i_{dGC} must be reduced to increase voltage V_{DC} , i.e., active power P_{GC} transmitted to the grid should be reduced.

Most of the simulation parameters are the same as shown in Table 3 for $n = 5$; in Table 6, the parameters that changed compared to Table 3 are included. Both the phase-to-phase wind farm output AC voltage, as the phase-to-phase onshore grid AC voltage are 25 kV rms. HVDC transmission line has a DC voltage of 46.2 kV.

Table 6
Simulation parameters for MMC connected to the wind farm (WF-MMC), and the MMC connected to the grid (GC-MMC) (only the parameters that are different from those in Table 3 were included).

	WF-MMC	GC-MMC
V_{DC}	46.2 kV	46.2 kV
C_{DC}	50 μ F	50 μ F
R	2 Ω	2 Ω
$V_{AC,ph-to-ph,rms}$	25 kV	25 kV
L_c	12 mH	12 mH
P^*	0–9 MW	
Q^*	0	–5 MVAR
$k_{p,P}$	$6.67 \cdot 10^{-6}$	
$k_{i,P}$	0.00667	
$k_{p,Q}$	$-6.67 \cdot 10^{-6}$	0
$k_{i,Q}$	–0.00667	–0.00667
$k_{p,VDC}$		–1.2
$k_{i,VDC}$		–4

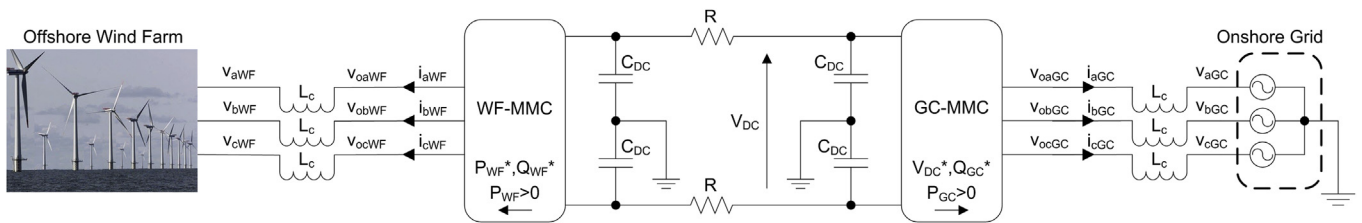


Fig. 26. HVDC transmission scheme between the offshore wind farm and the onshore grid.

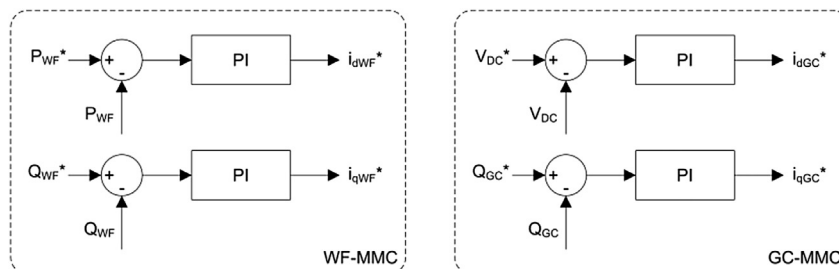


Fig. 27. PI regulators of the WF-MMC and the GC-MMC.

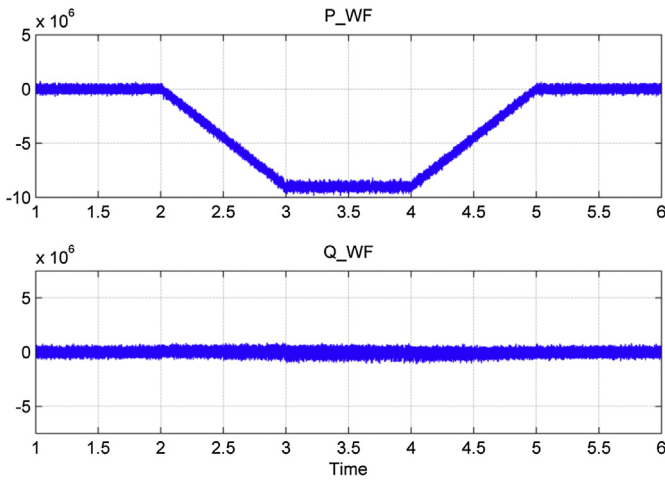


Fig. 28. Active P_{WF} and reactive Q_{WF} power exchanged between the WF-MMC and the wind farm.

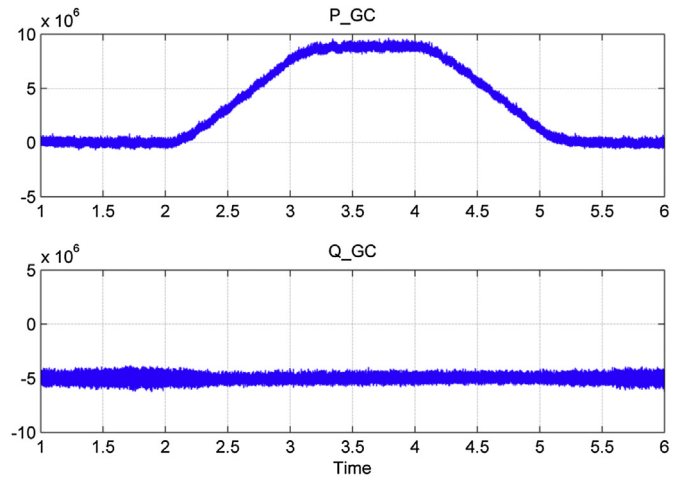


Fig. 31. Active P_{GC} and reactive Q_{GC} power exchanged between the GC-MMC and the grid.

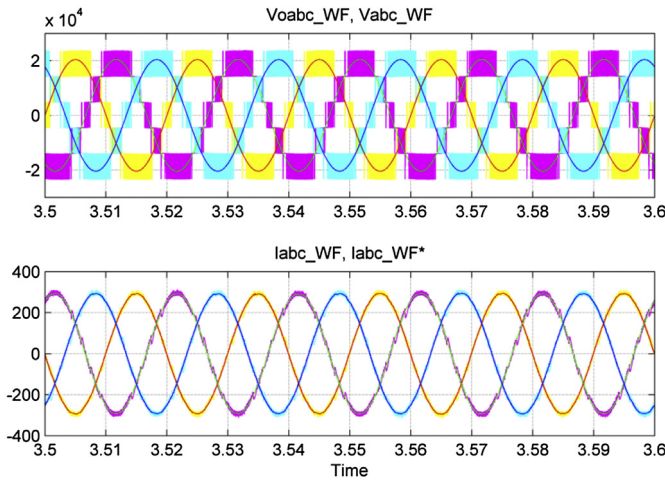


Fig. 29. WF-MMC voltages v_{oabcWF} , wind farm voltages v_{abcWF} , WF-MMC currents i_{abcWF} and reference values of the WF-MMC currents i_{abcWF}^* .

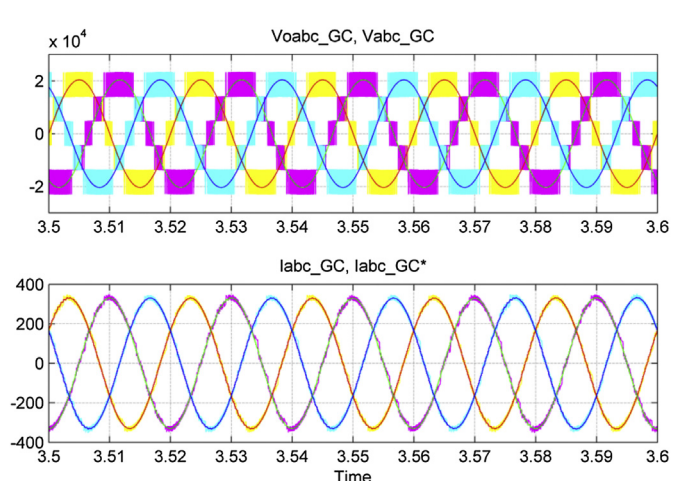


Fig. 32. GC-MMC voltages v_{oabcGC} , grid voltages v_{abcGC} , GC-MMC currents i_{abcGC} and reference values of the GC-MMC currents i_{abcGC}^* .

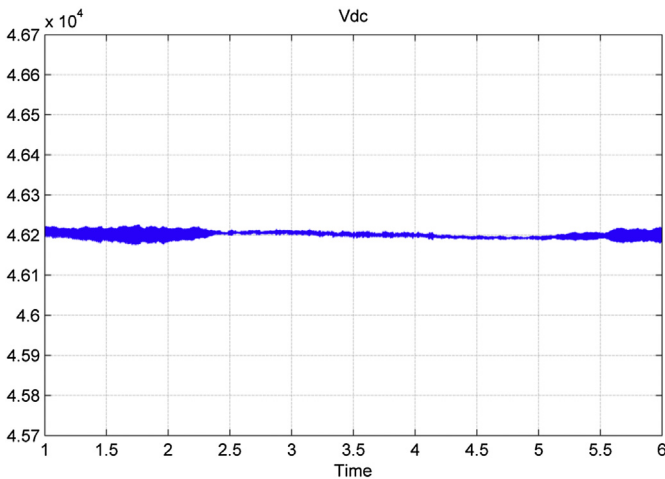


Fig. 30. DC voltage of the GC-MMC.

Active power P_{WF} profile of the wind farm, which consists of two ramps and a section of 9 MW constant power (Fig. 28), has been simulated. Power P_{WF} is negative in Fig. 28, because active power was considered positive when it leaves the MMC. Reactive power

Q_{WT} has been set to zero, but it would provide the reactive power required by the wind farm to the magnetization of the generators or to stabilize the AC voltage.

Control with constant current excitation of WT-MMC can be seen in Fig. 29. Converter AC output voltages v_{oabcWF} have six levels; these voltages are used to follow the reference of the phase currents i_{abcWF}^* with high accuracy.

The voltage V_{DC} regulator maintains the DC voltage around its reference value of 46.2 kV (Fig. 30). The GC-MMC converts the DC voltage to AC, and it transmits to the onshore grid the same profile of active power that the wind farm sends, and reactive power of -5MVAR (Fig. 31). The GC-MMC generates a six levels voltage v_{oabcGC} to follow the current references i_{abcGC}^* using the control with constant current excitation (Fig. 32).

8. Conclusions

In recent years, a great research effort is been done in using MMC in HVDC applications, including the development of simulation models, control of SM voltages, control of circulating currents, and converter control. In addition, the first commercial implementations of high power converters have been made.

A new control system for current control of MMC in HVDC applications has been proposed. It allows the grid connection currents to be controlled within error bands. Two novel approaches are used in this type of applications called: control with constant excitation and control with excitation proportional to the error. The objective is to keep the phase current around its reference value by choosing the appropriate output voltage level. Its salient features are:

- 1) The output current harmonics is well below the limits set by international standards.
- 2) The switching frequency of semiconductors is moderate and well suited for high power IGBTs.
- 3) The coupling inductance to the network is relatively small. Due to the use of a multilevel system, an output voltage of each phase can be chosen to generate a small coupling inductance voltage, so that the inductance can be relatively small.
- 4) The current controlled systems are simpler than the voltage controlled, as they do not have to transform the current references to voltage references in the control system.

The theoretical foundations and simulations results have been presented for the two types of current control. For control with constant excitation, a converter with 5 SMs per arm was used. However, for control with excitation proportional to the error, a converter with 10 SMs per arm was used, because this type of control is most appropriate when the number of levels of the output voltage is higher.

The simulation results show that the currents generated have very appropriate harmonic content, and include the graphs of the most important variables in the converters: the arm currents, the phase currents, the DC current, the circulating current, the capacitor voltages, the IGBT trigger signals and the active and reactive powers.

This type of control can be used for both converters, AC/DC and DC/AC, in an HVDC transmission, including the connection of offshore wind farms with onshore grid.

References

- [1] Serrano J, Burgos M, Riquelme J. Optimum design of transmissions systems for offshore wind farms including decision making under risk. *Renew Energy* 2013;59:115–27.
- [2] Bresesti P, Kling WL, Hendriks RL, Vailati R. HVDC connection of offshore wind farms to the transmission system. *IEEE Trans Energy Conv* 2007;22(1):37–43.
- [3] Decker JD, Woyte A. Review of the various proposals for the European offshore grid. *Renew Energy* 2013;49:58–62.
- [4] Chen Z, Guerrero JM, Blaabjerg F. A review of the state of the art of power electronics for wind turbines. *IEEE Trans Power Electron* 2009;24(8):1859–75.
- [5] Liserre M, Cárdenas R, Molinas M, Rodríguez J. Overview of multi-MW wind turbines and wind parks. *IEEE Trans Ind Electron* 2011;58(4):1081–95.
- [6] Flourentzou N, Agelidis VG, Demetriades GD. VSC-based HVDC power transmission systems: an overview. *IEEE Trans Power Electron* 2009;24(3):592–602.
- [7] Montilla-DJesus M, Santos-Martin D, Arnaltes S, Castronuovo ED. Optimal reactive power allocation in an offshore wind farms with LCC-HVDC link connection. *Renew Energy* 2012;40(1):157–66.
- [8] Lesnicar A, Marquardt R. An innovative modular multilevel converter topology suitable for a wide power range. In: *Proc. Power Tech Conference*; Jun. 2003. p. 23–6. Bologna-Italy.
- [9] Rohner S, Bernet S, Hiller M, Sommer R. Modulation, losses, and semiconductor requirements of modular multilevel converters. *IEEE Trans Ind Electron* 2010;57(8):2633–42.
- [10] Zhang M, Huang L, Yao W, Lu Z. Circulating harmonic current elimination of a CPS-PWM-based modular multilevel converter with a plug-in repetitive controller. *IEEE Trans Power Electron* 2014;29(4):2083–97.
- [11] Du S, Liu J. A study on dc voltage control for chopper-cell-based modular multilevel converters in D-STATCOM application. *IEEE Trans Power Deliv* 2013;28(4):2030–8.
- [12] Mohammadi HP, Tavakoli Bina M. A transformerless medium-voltage STATCOM topology based on extended modular multilevel converters. *IEEE Trans Power Electron* 2011;26(5):1534–45.
- [13] Abildgaard EN, Molinas M. Modelling and control of the modular multilevel converter (MMC). *Energy Procedia* 2012;20:227–36.
- [14] Mahimkar N. G. Persson, C. Westerlind, HVDC technology for large scale offshore wind connections. In: *Presented at Smartelec*; 2013, April 16. Vadodara, India.
- [15] Alstom Grid, HVDC-VSC: transmission technology of the future. Available from: <http://www.alstom.com/Global/Grid/Resources/Documents/Smart%20Grid/HVDC-VSC%20transmission%20technology%20of%20the%20future%20-%20Think%20Grid%20n%C2%B08%20.pdf?epslanguage=en-GB>.
- [16] Davies M, Dommaschk M, Dorn J, Lang J, Retzmann D, Soerangr D. HVDC PLUS – basics and principle of operation. Available from: <http://www.energy.siemens.com/br/pool/br/transmissao-de-energia/transformadores/hvdc-plus-basics-and-principle-of-operation.pdf>.
- [17] Marquardt R. Modular multilevel converter: an universal concept for HVDC-networks and extended DC-bus-applications. In: *Proceedings on international power electronics conference (IPEC)*, Sapporo, Japan; 21–24 Jun. 2010. p. 502–7.
- [18] Bergna G, Berne E, Egrot P, Lefranc P, Arzandé A, Vannier JC, et al. An energy-based controller for HVDC modular multilevel converter in decoupled double synchronous reference frame for voltage oscillation reduction. *IEEE Trans Ind Electron* 2013;60(6):2360–71.
- [19] Saeedifard M, Irvani R. Dynamic performance of a modular multilevel back-to-back HVDC system. *IEEE Trans Power Deliv* 2010;25(4):2903–12.
- [20] Hagiwara M, Akagi H. Control and experiment of pulsewidth-modulated modular multilevel converters. *IEEE Trans Power Electron* 2009;24(7):1737–46.
- [21] Qin J, Saeedifard M. Predictive control of a modular multilevel converter for a back-to-back HVDC system. *IEEE Trans Power Deliv* 2012;27(3):1538–47.
- [22] Deng F, Chen Z. A control method for voltage balancing in modular multilevel converters. *IEEE Trans Power Electron* 2014;29(1):66–76.
- [23] Saad H, Peralta J, Denetière S, Mahseredjian J, Jatskevich J, Martinez JA, et al. Dynamic averaged and simplified models for MMC-based HVDC transmission systems. *IEEE Trans Power Deliv* 2013;28(3):1723–30.
- [24] Peralta J, Saad H, Denetière S, Mahseredjian J, Nguefeu S. Detailed and averaged models for a 401-level MMC–HVDC system. *IEEE Trans Power Deliv* 2012;27(3):1501–8.
- [25] Gnanarathna UN, Gole AM, Jayasinghe RP. Efficient modeling of modular multilevel HVDC converters (MMC) on electromagnetic transient simulation programs. *IEEE Trans Power Deliv* 2011;26(1):316–24.
- [26] Qin J, Saeedifard M. Reduced switching-frequency voltage-balancing strategies for modular multilevel HVDC converters. *IEEE Trans Power Deliv* 2013;28(4):2403–10.
- [27] Song Q, Liu W, Li X, Rao H, Xu S, Li L. A steady-state analysis method for a modular multilevel converter. *IEEE Trans Power Electron* 2013;28(8):3702–13.
- [28] Moon JW, Kim CS, Park JW, Kang DW, Kim JM. Circulating current control in MMC under the unbalanced voltage. *IEEE Trans Power Deliv* 2013;28(3):1952–9.
- [29] Li X, Song Q, Liu W, Rao H, Xu S, Li L. Protection of nonpermanent faults on DC overhead lines in MMC-based HVDC systems. *IEEE Trans Power Deliv* 2013;28(1):483–90.
- [30] Tu Q, Xu Z. Impact of sampling frequency on harmonic distortion for modular multilevel converter. *IEEE Trans Power Deliv* 2011;26(1):298–306.
- [31] Guan M, Xu Z. Modeling and control of a modular multilevel converter-based HVDC system under unbalanced grid conditions. *IEEE Trans Power Electron* 2012;27(12):4858–67.
- [32] Arruda LN, Silva SM, Filho BJC. PLL structures for utility connected systems. In: *Proc. industry applications conference*; 30 Sept.–1 Oct. 2001. Chicago, USA.
- [33] Blaabjerg F, Teodorescu R, Liserre M, Timbus AV. Overview of control and grid synchronization for distributed power generation systems. *IEEE Trans Ind Electron* 2006;53(5):1398–409.